NANO LETTERS

pubs.acs.org/NanoLett

Letter

Elucidating the Effects of LiF on Lithium Metal Anodes

Mun Sek Kim, Jingyang Wang, Wenbo Zhang, Philaphon Sayavong, Zewen Zhang, Solomon T. Oyakhire, Sanzeeda Baig Shuchi, Sang Cheol Kim, Yi Cui, Yuelang Chen, Zhiao Yu, Huaxin Gong, Rong Xu, Junyoung Lee, Il Rok Choi, Jun Ho Lee, Kristin A. Persson, Jian Qin, Zhenan Bao,* and Yi Cui*

Cite This: *Nano Lett.* 2025, 25, 14625−14634

Read Online

ACCESS | Metrics & More | Article Recommendations | Supporting Information

ABSTRACT: LiF is widely recognized as a crucial component of a solid-electrolyte interphase (SEI) for Li metal anodes. However, the roles of LiF in the SEI remain elusive. Herein, we examined the evolution of SEI influenced by LiF and identified distinct features that elucidate functional characteristics of LiF for Li metal anodes. Through comprehensive empirical and theoretical analyses, we found that LiF enriches Li_2O within the SEI, forms LiF/Li_2O interfaces, exhibits non-negligible solubility with spontaneous dissolution-reprecipitation behavior in the electrolyte, and works synergistically with Li_2O. These findings shed light on the effects of LiF on Li metal anodes and the arrangement characteristic of LiF within the SEI. By integrating key discoveries regarding LiF, a projected working mechanism for LiF is illustrated. Overall, our study on LiF provides valuable insights that advance the understanding of the SEI and interphase nanostructures, contributing to the development of more reliable and practical Li metal batteries.

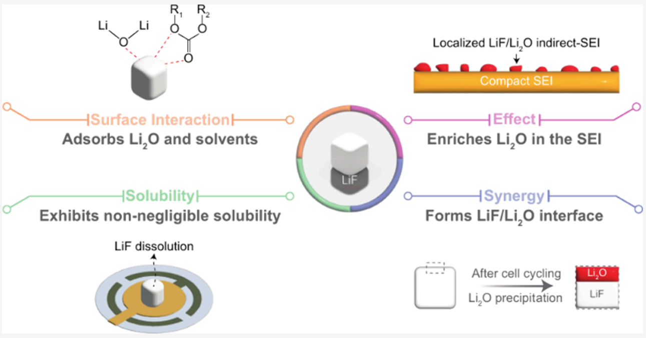

KEYWORDS: *Lithium fluoride, LiF, Lithium oxide, Solid electrolyte interphase, SEI, Lithium metal anode*

Lithium fluoride (LiF) is widely perceived as a beneficial inorganic solid-electrolyte interphase (SEI) component for lithium metal (Li^0) anodes.[1−4] Yet, its precise role in SEIs remains equivocal due to uncertainties regarding its physicochemical properties,[5−7] spatial distribution,[4,8] and generalized performance benefits.[3,9] Despite these ambiguities, LiF continues to be a key descriptor for SEIs and electrolyte design for high-performance Li^0 batteries.[3,4] As such, elucidating the effects of LiF on Li^0 anodes is crucial for devising strategies to precisely tailor SEI nanostructures and chemistries for developing efficient and reversible Li^0 batteries.[1]

Although the high bulk modulus,[10,11] interfacial energy,[12] redox stability,[13] and low electrical conductivity[14] of LiF within SEIs are known to be advantageous for suppressing metal dendrite ramification,[4] the poor lithium-ion (Li^+) conductivity of LiF[14] (ranging from 10^{-13} to 10^{-14} S cm^{-1})[4] complicates direct correlations between LiF content and the performance of Li^0 anodes,[5−7,15,16] prompting further investigation into the major roles of LiF in SEIs.[1,4,9] Moreover, the spatial distribution of LiF within the compact-SEI, a passivation layer directly interfacing Li^0, remains debatable. Traditionally, LiF has been identified using X-ray photoelectron spectroscopy (XPS).[4] While XPS provides high resolution in the out-of-plane direction, its limited in-plane spatial resolution when characterizing heterogeneous and rough interphases on Li^0 anodes has led to inaccuracies in determining the spatial arrangement of LiF within SEIs.[4,8,9] To address this challenge, cryogenic transmission electron microscopy (cryo-TEM) has been employed to directly observe SEI nanostructures on Li^0 anodes.[8,17] Although depth-profiling XPS analysis indicated the presence of LiF in the inner regions of the compact-SEI,[4,8,9] cryo-TEM revealed a notable absence of LiF within the compact-SEI.[8,18−25] Despite LiF being seldom found, when observed, it frequently coexists with and interfaces alongside Li_2O within the compact-SEI.[16,26−30] Given the nondominant presence of LiF in the compact-SEI, the extent to which Li^0 anodes directly benefit from the passivating properties of LiF alone has come into question.[8,9] Additionally, LiF is often found as part of the indirect-SEI,[8,19,22−24] an extended form of SEI sporadically distributed as particulates at the compact-SEI/electrolyte interface, passivated by Li_2O.[8,19,21,25] The rationales

Received: July 7, 2025
Revised: September 21, 2025
Accepted: September 24, 2025
Published: September 29, 2025

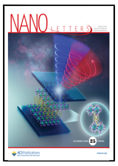

ACS Publications

https://doi.org/10.1021/acs.nanolett.5c03437

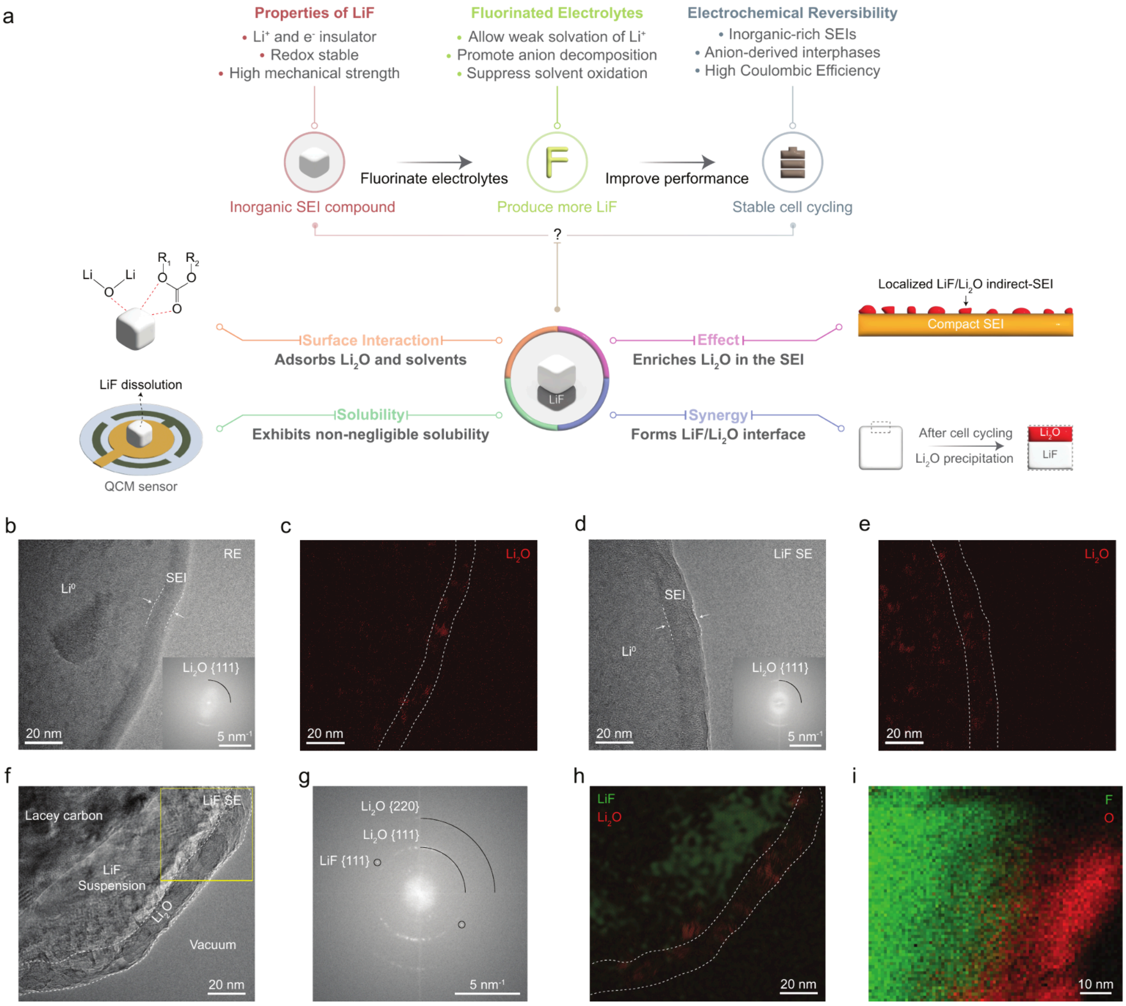

Figure 1. Summary of LiF and interphase analysis on Li^0 and LiF suspension. (a) Schematic illustration outlining the motivation behind LiF and summarizing new findings of LiF in this work. (b) Cryo-HRTEM image of the compact-SEI on electrodeposited Li^0 with RE. The inset represents FFT of (b), showing Li_2O {111} diffraction pattern. (c) Inverse FFT of the inset in (b), showing Li_2O {111}. (d) Cryo-HRTEM image of the compact-SEI on electrodeposited Li^0 with LiF SE. The inset represents FFT of (d), showing Li_2O {111} diffraction pattern. (e) Inverse FFT of the inset in (d), showing Li_2O {111} diffraction pattern. (f) Cryo-HRTEM image of the LiF suspension in LiF SE. The yellow square box represents the selected area for cryo-STEM EELS. (g) FFT of (f), showing LiF {111}, Li_2O {111}, and Li_2O {220} diffraction patterns. (h) Inverse FFT image of (g), displaying LiF {111} and Li_2O {111} in green and red, respectively. (i) Cryo-STEM EELS mapping of F and O for the region demarcated by the yellow box in (f).

behind its indirect-SEI arrangement, surface passivation with Li_2O, and functional characteristics have remained puzzling.

The initial drive behind developing fluorinated electrolytes was centered on forming LiF-rich SEIs on Li^0 anodes.[3] As the body of research on fluorinated electrolytes for Li^0 batteries has expanded significantly since then,[31−34] fluorinated electrolytes have been recognized for creating a weakly solvating environment for Li^+, facilitating the reduction of anions, and suppressing solvent oxidation.[3,34] These specific features of fluorinated electrolytes induce inorganic-rich SEIs,[35−37] anion-derived (fluorinated) interphase compounds,[3] and high Coulombic efficiency (CE)[38] for Li^0 anodes, which have become direct indicators for enabling high-performance Li^0 batteries. However, the sporadic presence of LiF within SEIs[8,18−22,26,29,30] has prompted a reassessment of the roles LiF plays in SEIs. Although the initial endeavor to augment LiF content in SEIs spurred the development of highly successful fluorinated electrolytes,[3,34] it also exposed a significant gap in our understanding of LiF in intricate/dynamic SEIs on Li^0 anodes.[4,9]

Herein, a classic organic carbonate electrolyte and its altered version containing LiF suspension (Figure S1) were employed to investigate the impact of LiF on the SEI evolution of Li^0 anodes. The reference electrolyte (RE) of 1 M $LiPF_6$ in ethylene carbonate (EC):diethyl carbonate (DEC) (1:1 v/v) with 10 vol % fluoroethylene carbonate (FEC) was chosen to ensure our findings contribute to a deeper understanding based on prior SEI studies associated with LiF.[8,18,20,39−41] LiF suspension electrolyte (LiF SE) containing 15 wt % of 400 nm to 5 μm-sized LiF (Figure S2) in RE was used to maintain consistent bulk liquid electrolyte chemistry for the SEI analysis and to closely examine the effect of LiF on the SEI evolution for Li^0 anode. Based on empirical and theoretical investigations, we found that (1) LiF enriches Li_2O in the SEI (improving the performance of Li^0 anode), (2) the surfaces of LiF can serve as a favorable nucleation site for Li_2O (revealing the propensity of LiF to form LiF/Li_2O grain boundaries), (3) LiF exhibits non-negligible solubility and spontaneous dissolution-reprecipitation behavior in the electrolyte (impacting the spatial distribution of LiF within the SEI), and (4) the

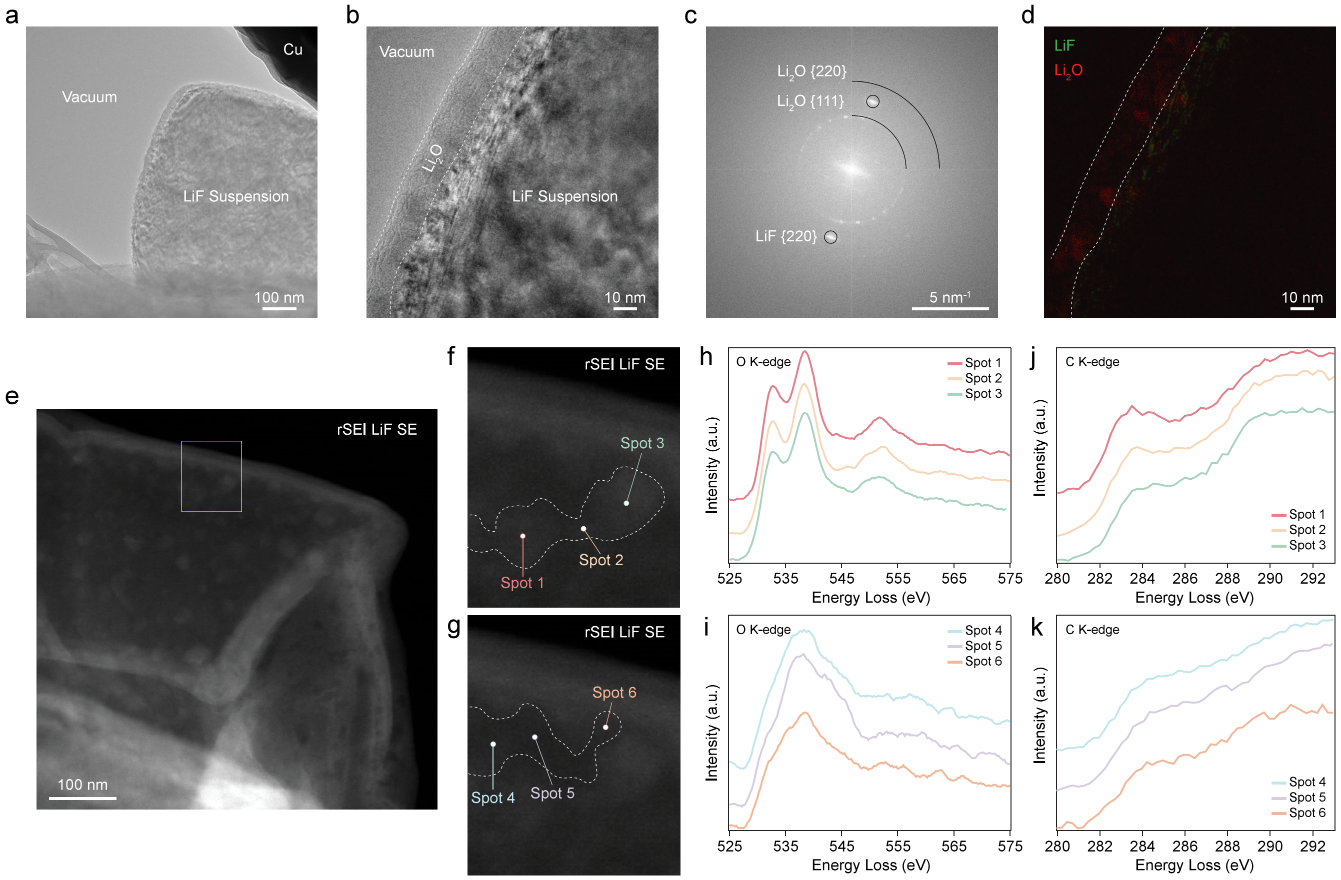

Figure 2. Analyses of LiF suspension and rSEI after cycling. (a,b) Low (a) and high (b) magnification cryo-HRTEM images of LiF suspension in LiF SE after cycling. The dashed white lines in (b) indicate Li_2O passivation layer on LiF suspension. (c) FFT of (b), showing LiF {220}, Li_2O {111}, and Li_2O {220} diffraction patterns. (d) Inverse FFT of (c), displaying LiF {220} and Li_2O {111} in green and red, respectively. (e) Cryo-STEM image of rSEI LiF SE. The yellow rectangle represents the selected area for the cryo-STEM EELS analysis. (f-g) Cryo-STEM EELS images of the bright (f) and dark (g) regions bordered with dashed lines corresponding to the yellow rectangle in (e). (h-i) Oxygen K-edge fine structure profiles of spot 1 ∼ 3, bright spots (h), and spot 4 ∼ 5, dark regions (i). (j-k) Carbon K-edge fine structure profiles of spot 1 ∼ 3, bright spots (j), and spot 4 ∼ 5, dark regions (k).

surfaces of LiF interact with Li_2O and electrolyte solvents (promoting the surface passivation of LiF with Li_2O and dissolution of LiF in the electrolyte). These key findings elucidate the uncertainties regarding the effects of LiF on Li^0 anodes (Figure 1a).

To assess the effects of LiF on the SEI evolution, the compact-SEIs formed on the freshly electrodeposited Li^0 with RE (Figure 1**b,c**) and LiF SE (Figure 1**d,e**) were examined by cryo-TEM. Upon analyzing high-resolution cryo-TEM (cryo-HRTEM) images of electrodeposited Li^0 with RE, the Fast Fourier Transform (FFT) diffraction pattern corresponding to Li_2O {111} (inset of Figure 1b) was observed. Although the inverse FFT of Figure 1b (Figure 1c) confirms the presence of Li_2O in the SEI, no observable diffraction from LiF lattices was detected, which agrees with previous findings[8,20,39] (Note S1). The cryo-HRTEM analysis of the electrodeposited Li^0 with LiF SE (Figure 1d) was conducted to probe the relative difference in the SEIs. A comparison of the FFT patterns shown in the inset of Figure 1d (LiF SE) and Figure 1b (RE) reveals a stronger Li_2O diffraction intensity for LiF SE. The inverse FFT of Figure 1d (Figure 1e) shows an enhanced Li_2O distribution compared to Figure 1c, indicating that LiF SE promoted the enrichment of Li_2O in the SEI. However, diffraction from LiF lattices was still absent for LiF SE (discussed later).

Considering the observed effect of LiF in increasing the relative abundance of Li_2O within the SEI (Figure 1**d,e**), the LiF suspension in LiF SE, identical sample in Figure 1d, was examined using cryo-TEM (Figure 1**f,g**) and scanning cryo-TEM electron energy loss spectroscopy (cryo-STEM EELS) (Figure 1**h,i**) to determine whether LiF remains inert, as it is typically considered.[4,36] The cryo-HRTEM image in Figure 1f reveals that the LiF suspension is passivated by Li_2O. This was further verified by the FFT and inverse FFT analysis in Figure 1**g,h**, which exhibited pronounced diffraction patterns for LiF {111}, Li_2O {111}, and Li_2O {220} planes. In addition, a clear boundary between F and O, indicating the LiF/Li_2O interface, was detected through cryo-STEM EELS in Figure 1i. Although the Li_2O passivation on the surfaces of LiF[8,19,21,25] and the coexistence of LiF/Li_2O in SEIs[16,26−30] have been observed, these phenomena have largely been overlooked and inadequately discussed (Note S2). Drawing on the observed effects of LiF in forming Li_2O passivation (Figure 1**f-i**), enriching Li_2O in the SEI (Figure 1**b-e**), and corroborating evidence of LiF/Li_2O from the earlier studies,[8,16,19,21,25−30] we found that LiF has a strong tendency to form LiF/Li_2O interface.

To investigate the surface passivation mechanism of LiF and the role of LiF in Li_2O enrichment in the SEI, the LiF suspension and a residual SEI (rSEI) formed after ten

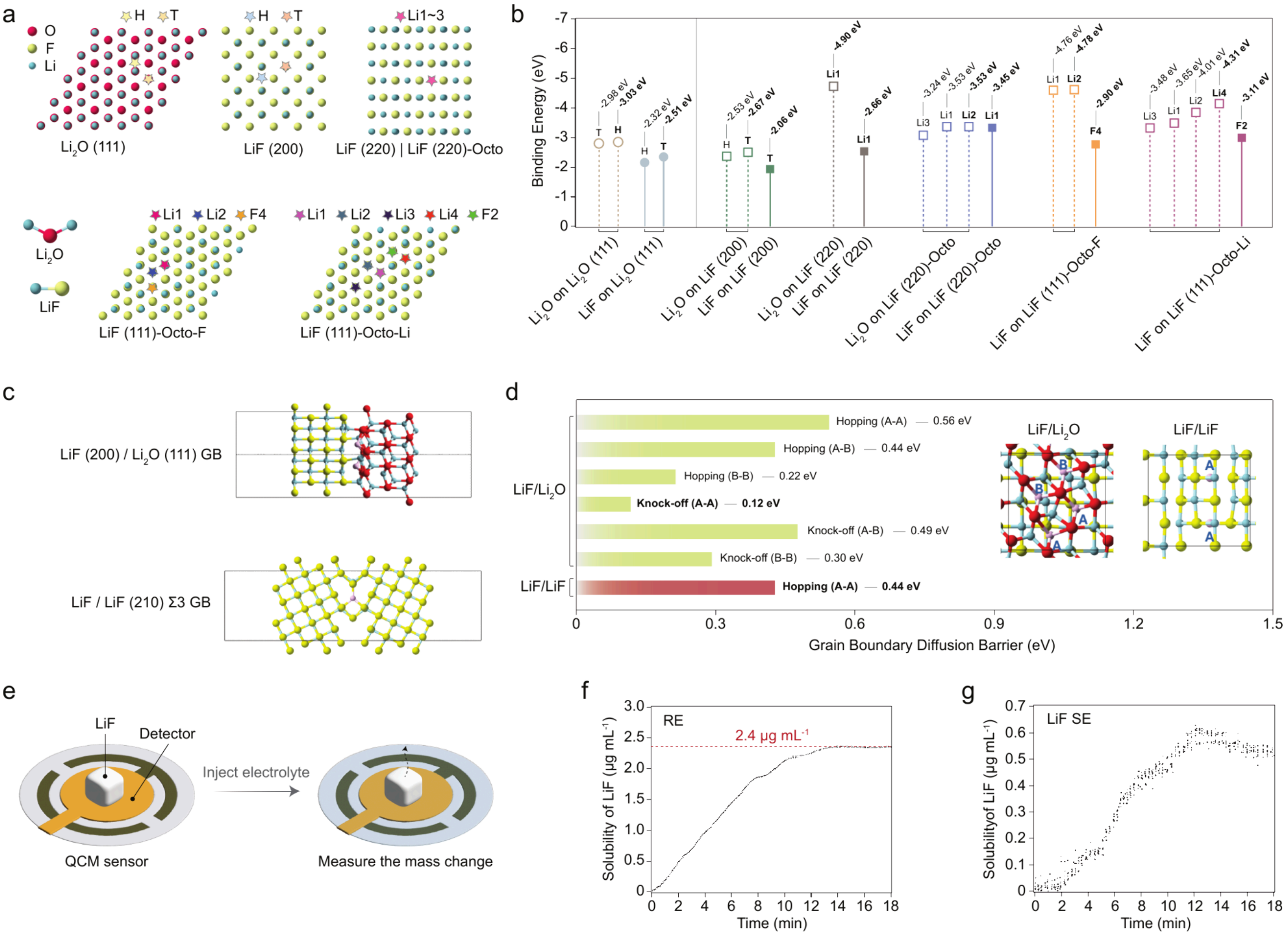

Figure 3. Properties of LiF. (a) Crystal structures of Li_2O (111), LiF (200), LiF (220), LiF (220)-Octo, LiF (111)-Octo-F, and LiF (111)-Octo-Li slabs used for Li_2O and LiF molecular binding analysis. The hollow (H), top (T), and Li1 ∼ 4, indicated by the filled stars, represent specific binding sites for Li_2O and LiF molecules. (b) Binding energies of Li_2O and LiF molecules onto the binding sites shown in (a). The surface adsorption of Li_2O molecule is indicated in the dashed line and open symbol, whereas the surface adsorption of LiF molecule is represented by the solid line and filled symbol. The circle and square symbols signify Li_2O and LiF surfaces, respectively, which the Li_2O and LiF surfaces are separated by the solid gray line. The most favorable binding site and corresponding binding energy for each of Li_2O or LiF surfaces are highlighted in bold text. (c) Schematics of a LiF (200)/Li_2O (111) grain boundary (GB) and a LiF/LiF (210) Σ3 GB. Red, yellow, and blue spheres denote O, F, and Li atoms, respectively. (d) Activation energy barriers for Li diffusion in the LiF/Li_2O and LiF/LiF GBs. The plausible GB diffusion pathways for a Li atom are illustrated in the inset of (d). The blue and red arrows indicate hopping and knock-off mechanisms, and the pink spheres with letters denote high symmetry sites inside the LiF/Li_2O and LiF/LiF GBs. (e) Schematic illustration of LiF solubility measurement using the QCM. (f,g) LiF solubility profile in RE (f) and LiF SE (g).

complete cycles of Li^0 plating and stripping with LiF SE were characterized (Figure 2). The characterizations from cryo-HRTEM (Figure 2**a**,**b**) confirm that the LiF suspension remains passivated with Li_2O, as evidenced by the FFT diffraction patterns in Figure 2c and the inverse FFT in Figure 2d, demonstrating that Li_2O on the LiF surface stays intact and persists throughout cell cycling. Based on the Li_2O passivation mechanism analysis (Note S3), it was found that Li_2O passivation on LiF surfaces occurs via physical precipitation.

To understand the nanoscopic origin of the spatial distribution and enrichment of Li_2O in rSEI LiF SE (Note S4), cryo-STEM EELS characterizations were performed (Figure 2**e**-**k**). From the cryo-STEM image in Figure 2e, rSEI LiF SE portrayed distinct bright spots that differed in contrast. The cryo-STEM EELS fine structures were scanned within the designated area, demarcated by a yellow rectangle in Figure 2e, to probe chemistry information. Then, three spots were sampled each for both bright (Figure 2f) and dark (Figure 2g) regions. For the bright regions (Spot 1 ∼ 3), the corresponding fine structure of the O K-edge (Figure 2h) closely resembles the STEM EELS signal of Li_2O,[19] whereas the dark regions (Spot 4−6) display a comparatively weaker Li_2O signal in the O K-edge fine structure (Figure 2i). On the other hand, the C K-edge fine structures for both bright (Figure 2j) and dark (Figure 2k) regions showed minimal variation, compared to the pronounced differences in the O K-edge fine structure in Figure 2h and Figure 2i. This suggests that the localized bright spots observed in Figure 2e are Li_2O-rich areas.

Furthermore, the C K-edge fine structure in the bright regions (Figure 2j) aligns closely with the fine structure of the C K-edge observed for LiF in contact with the compact-SEI,[19] indicating the presence of LiF in the bright regions. To verify this, the F K-edge fine structure was measured in both bright and dark regions (Figure S3). In the bright region, the F K-edge fine structure resembles that of LiF,[42] demonstrating the

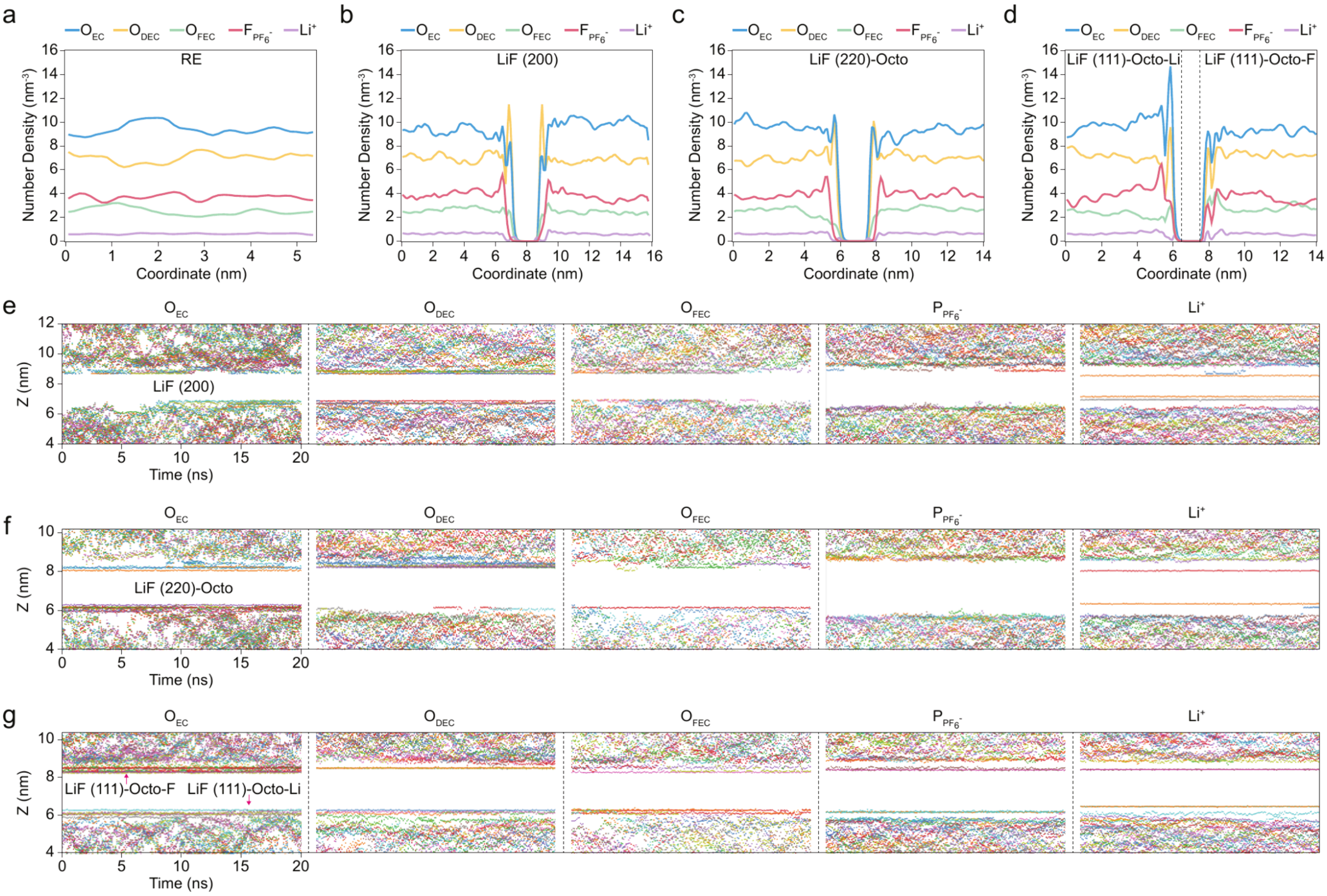

Figure 4. Molecular dynamics (MD) simulation of molecular interactions at the LiF/electrolyte interface. (a-d) Number density profiles of EC (O_{EC}), DEC (O_{DEC}), FEC (O_{FEC}), PF_6^- (F_{PF6}), and Li^+ in RE with no surface (a), near the LiF (200) surface (b), near the LiF (220)-Octo surface (c), and near the LiF (111)-Octo-F and LiF (111)-Octo-Li surfaces (d). (e-g) z-coordinate trajectories of O_{EC}, O_{DEC}, O_{FEC}, P_{PF6}, and Li^+ near the LiF (200) surface (e), LiF (220)-Octo surface (f), and LiF (111)-Octo-F surface and LiF (111)-Octo-Li surface (g). Each colored dot represents a unit of EC, DEC, FEC, PF_6^-, and Li^+ at a given time. The vertical axis of the plots illustrates the *z*-axis (height in nanometers) in the simulation box; the horizontal axis shows the simulation time in nanoseconds.

presence of LiF along with Li_2O. Overall, cryo-STEM EELS fine structure analysis elucidates that the localized bright spots in Figure 2e correspond to LiF/Li_2O, which closely resemble the previously observed LiF/Li_2O core−shell nanostructure identified as the indirect-SEI.[8] To this point, we have empirically identified three key effects of LiF: (1) the propensity for LiF to interface with Li_2O, forming LiF/Li_2O interface (Figure 1**f-i** and Figure 2**a-d**); (2) Li_2O passivation on the surfaces of LiF, occurring through the precipitation mechanism (Note S3); and (3) the enrichment of Li_2O within the compact-SEI (Figure 1**d,e**) and LiF/Li_2O indirect-SEI (Figure 2**e-k**), with a lack of LiF presence in the compact-SEI on Li^0 (Figure 1**b-e**).

To elucidate the observed effects of LiF, Li_2O binding affinity, Li grain boundary diffusion, solubility, and dissolution−precipitation behavior for LiF were interrogated through density functional theory (DFT) and quartz crystal microbalance (QCM) analyses (Figure 3). For DFT analysis, LiF (200), LiF (220), LiF (220)-Octo, LiF (111)-Octo-F, and LiF (111)-Octo-Li were selected (Note S5). In determining the propensity of LiF to interface with Li_2O, the molecular binding energies of Li_2O on LiF surfaces were calculated (Figure 3**a,b**). For benchmarking, two reference cases were considered: (1) Li_2O and LiF molecules binding onto Li_2O (111) surface[40] and (2) Li_2O and LiF molecules binding onto LiF surfaces. In Figure 3a, the surface binding sites (Hollow (H), Top (T), and Li1 ∼ 4, F2, and F4) are illustrated, and corresponding initial and final binding configurations of LiF and Li_2O are provided in Figure S4 and Figure S5. In the former case, the more negative binding energies of Li_2O compared to LiF on Li_2O (111) surface (Figure 3b) demonstrate that the Li_2O surface has a stronger propensity to bind with itself rather than with LiF. Given the polycrystalline nature of LiF,[8,29,30,43,44] all relevant LiF surfaces were evaluated to determine the general binding affinity of Li_2O (Figure 3b). In the latter case, all LiF surfaces exhibited a higher binding affinity for Li_2O than for LiF, as evidenced by the more negative binding energies for Li_2O. This trend demonstrates that Li_2O adsorption is thermodynamically more favorable on the surfaces of LiF (Note S6). Collectively, the results in Figure 3b elucidate a unique role of LiF: its ability to form LiF/Li_2O interface, thereby the grain boundaries, where LiF surfaces can act as favorable nucleation/interaction sites for Li_2O.

To understand the potential benefit of LiF/Li_2O indirect-SEI (Figure 2e) and LiF/Li_2O interface (LiF being interfaced[16,26−30] with or passivated[8,19,21,25] by Li_2O), the Li diffusion barrier across LiF/Li_2O grain boundary was investigated to observe the effect of the LiF/Li_2O interface on Li transport. For comparative analysis, grain boundaries (GBs) of both LiF/Li_2O and LiF/LiF were constructed

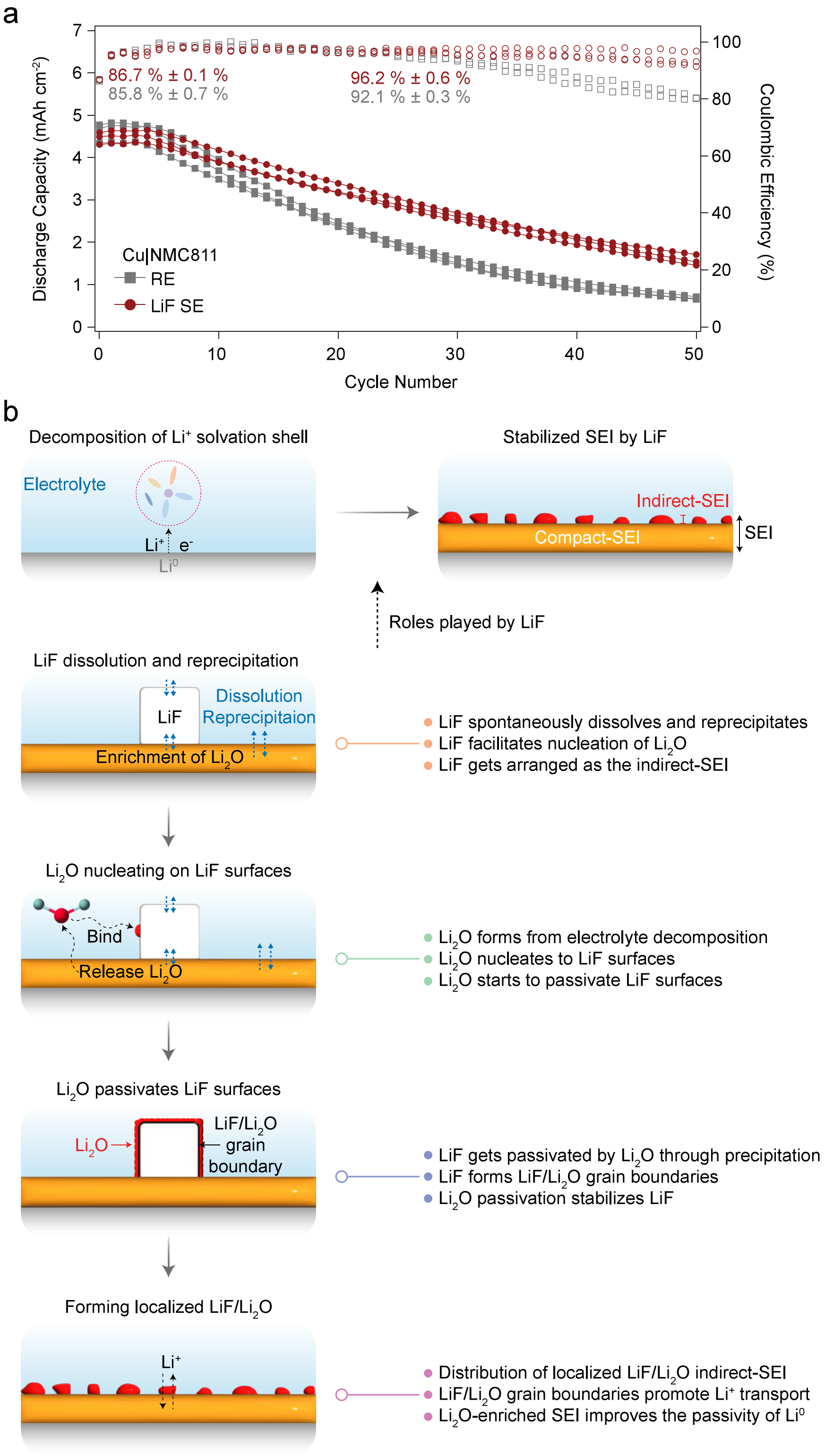

Figure 5. Full cell cycling analysis and working mechanism of LiF for Li^0 anode. (a) Cu|NMC811 anode-less cell cycling performances with RE and LiF SE. The Cu|NMC811 cells were charged up to 4.2 V vs Li^+/Li with a current density of 0.4 mA cm^{-2}, and constant voltage charging was applied at 4.3 V vs Li^+/Li with a cutoff current of 0.04 mA cm^{-2}. Then the cells were galvanostatically discharged from 4.3 to 3 V vs Li^+/Li with a current density of 0.8 mA cm^{-2}. The filled and open symbols represent the areal discharge capacity and CE. (b) Schematic illustrations of the proposed working mechanism of LiF for Li^0 anode.

(Figure 3c), and the corresponding Li grain boundary diffusion barriers were calculated (Figure 3d and Figure S6). Activation energy barriers for diffusion pathways in LiF (200)/Li_2O (111) GB are 0.56 eV, 0.44 eV, 0.22 eV for hopping mechanisms (A-A, A-B, B−B) and 0.12 eV, 0.49 eV, 0.30 eV for knock-off mechanisms (A-A, A-B, B−B). Among these pathways, three of them are more kinetically favorable compared with hopping diffusion in LiF/LiF (210) Σ3 GB

(0.44 eV). These findings suggest that interfacing LiF with Li_2O, equivalent to the LiF/Li_2O GB, can facilitate Li transport, aligning with the previous study.[45] Based on the presence of LiF/Li_2O indirect-SEI nanostructure (Figure 2e) and the disposition for LiF to form LiF/Li_2O interface (Figure 3b), it can be more relevant that LiF facilitates Li diffusion across the SEI primarily through its role in forming the LiF/Li_2O grain boundary, rather than via LiF surfaces alone[46,47] (Note S7).

Although the distribution of LiF/Li_2O indirect-SEI (Figure 2e), the interfacing mechanism of LiF with Li_2O (Figure 2**a**-**d**, Figure 3**a**,**b**, **and** Note S3), and the benefit of LiF/Li_2O interface (Figure 3d) have been examined, the lack of LiF presence within the compact-SEI (Figure 1**b**-**e**) remains a puzzling phenomenon (Note S8). Since SEIs are known to be soluble,[48,49] permeable to electrolytes,[18] and extremely thin,[36] the solubility and dissolution/precipitation behavior of LiF in the electrolyte can affect the spatial arrangement of LiF within the SEI. To investigate this, QCM was used to probe the solubility and dissolution/precipitation behavior of LiF (Figure 3e). According to the LiF dissolution in RE depicted in Figure 3f, the solubility of LiF was approximately 2.4 μg mL^{-1}, which equates to a concentration of 0.093 mM. The solubility was determined at the point where the LiF solubility leveled off at a plateau of around 14 min, indicated by the dashed red line in Figure 3f (Note S9). This value estimates that 30 μm of a LiF cube can dissolve in 30 μL of RE, which is a typical lean electrolyte amount for making coin cells. Importantly, this dissolution amount of LiF is non-negligible, considering the thin length scale[36] and low LiF contents[16] of SEIs.

Furthermore, the dynamics of LiF dissolution behavior in the LiF-saturated electrolyte (LiF SE) were probed by the QCM (Figure 3g). In Figure 3g, the LiF solubility profile reveals that LiF on the QCM detector dissolves away (up to 12 min), then redeposits (after 12 min). This phenomenon occurs in the LiF-saturated electrolyte due to the cyclic process of spontaneous LiF dissolution and reprecipitation, also known as Ostwald ripening. Such observations suggest that LiF can spontaneously dissolve (migrate away) and reprecipitate (redeposit elsewhere) at equilibrium (Note S10). Considering these dynamics of LiF dissolution behavior in the electrolytes, the dissolution of LiF can play a critical role in dictating its spatial distribution within the SEIs (Note S11). Collectively, the non-negligible solubility (Figure 3f) and spontaneous dissolution-reprecipitation of LiF (Figure 3g) in the electrolyte, thus, provide critical insights into the lack of LiF presence within the compact-SEI[8,18−25] (Figure 1**b**-**e**).

To illustrate the surface interactions of LiF with electrolyte species in RE, the number density profiles of species in an RE with no surface (Figure 4a), near the LiF (200) surface (Figure 4b), near the octopolar-reconstructed LiF (200) (LiF (220)-Octo) surface (Figure 4c), and near the octopolar-reconstructed LiF (111) (LiF (111)-Octo) surfaces (Li-top and F-top) (Figure 4d) were examined with molecular dynamics (MD) simulations (Figure S7). After carefully analyzing the LiF/electrolyte interface, we found that solvents (particularly EC and DEC) and Li^+ in the electrolyte were strongly interacting with LiF surfaces (Note S12). To visualize the surface interactions at the LiF/electrolyte interface, z-coordinate trajectories of each electrolyte entity (O_{EC}, O_{DEC}, O_{FEC}, P_{PF6}, and Li^+) at the surfaces of LiF (200) (Figure 4e), LiF (220)-Octo (Figure 4f), and LiF (111)-Octo (Figure 4g) were plotted (Figure S8). From the trajectory plots in Figure 4**e**-**g**, the line profiles, indicative of surface adsorptions, were evidently delineated for the solvents and Li^+ at LiF surfaces (Note S13), in which the results reflect a congruent trend seen in the number density profiles in Figure 4**a**-**d**. The line profile analysis, therefore, unveils the unique trait of LiF: the capability of LiF to adsorb solvents and Li^+ onto its surfaces. The adsorption of solvent molecules onto LiF surfaces observed in the MD simulations elucidates its non-negligible dissolution (Figure 3f) and spontaneous dissolution-reprecipitation (Figure 3g) in RE, which can impact the lack of LiF presence in the compact-SEI[8,18−25] (Figure 1**b**-**e**) and the placement of LiF around the indirect-SEI regions[8,19,22−24] (Figure 2e). Furthermore, it is conceivable that LiF's ability to surface-adsorb Li^+ (Figure 4**e**-**g**) and create a weakly solvating environment (Note S14) simultaneously contributes to facilitating Li^+ transport[50] by rectifying solvated Li^+ through the LiF/Li_2O[45] grain boundaries (Figure 2e and Figure 3d).

To assess the electrochemical attributes of the SEI in Figure 2e, the anode-less cells (Cu|$LiNi_{0.8}Mn_{0.1}Co_{0.1}$-NMC811), each infused with 30 μL of RE and LiF SE, underwent cycling between 3 and 4.3 V vs Li^+/Li (Figure 5a). LiF SE exhibited a higher first cycle CE (LiF SE: 86.7% ± 0.1% and RE: 85.8% ± 0.7%), remaining cycle CE (LiF SE: 96.2% ± 0.6% and RE: 92.1% ± 0.3%), and capacity retention than those for RE (Figure 5a and Figure S9). Upon examining the voltage profiles of RE and LiF SE (Figure S10), the increase of the cell overpotential after subsequent cycles was much suppressed for LiF SE. The enhanced cycling reversibility and lower overpotential build-up in anode-less cells point out that LiF-derived SEI enhances the functionality of Li^0 anodes. To validate this, CE and Li nucleation overpotential were measured in Li^0|Cu half cells with RE and LiF SE (Figure S11). LiF SE demonstrated an improved CE (LiF SE: 97.30% ± 0.21% and RE: 93.35% ± 2.15%), while showing negligible changes in Li nucleation overpotential (LiF SE: 77.53 mV ± 4.79 mV and RE: 76.57 mV ± 1.12 mV), where LiF exerted a minimal impact on the first Li^0 electrodeposition morphology (Figure S12). This electrochemical response of LiF suggests that its role in improving the electrochemical performances of Li^0 anode is contingent upon the formation of Li_2O, a process that necessitates electrochemical cycling to produce Li_2O through electrolyte decompositions (Note S15). Moreover, the interphase characteristics of pristine and electrodeposited Li^0 were systematically examined by electrochemical impedance spectroscopy and XPS (Figures S13−S15 and Tables S1−S8). It was found that LiF had minimal influence on pristine, uncycled Li^0 electrode (Note S16) but contributed to improved interphase passivity for electrodeposited Li^0 (Note S17). Collectively, the electrochemical analysis elucidates the potential synergy between LiF and Li_2O within the SEI, which contributes to the improved electrochemical performance of Li^0 anode.

By synthesizing key findings in this work, the projected working mechanism of LiF for Li^0 anode is illustrated in Figure 5b. Initially, the reactive Li^0 anode starts to get passivated by insoluble byproducts derived from decomposed Li^+ solvation shells in the electrolyte.[36] When LiF instantaneously precipitates within the SEI formation region, LiF facilitates the nucleation of Li_2O (Figure 1**d**,**e**), enabled by the high Li_2O binding affinity (Figure 3b). However, due to electrolyte penetration into the SEI,[18] electrolyte-exposed LiF can be dissolved (Figure 3f) and spontaneously reprecipitate elsewhere (Figure 3g), simultaneously leaving nucleated Li_2O

behind in the compact-SEI (Figure 1**d,e**). During spontaneous dissolution-reprecipitation of LiF around the SEI domain, LiF dissolves away (Figure 1**b-e**) within the compact-SEI due to its non-negligible solubility in the electrolyte (Figure 3f). These properties eventually lead LiF to be placed as the indirect-SEIs[8,22−25] (Figure 2e), at which Li_2O starts to passivate LiF surfaces (Figure 1**f-i** and Figure 2**a-d**) through the precipitation mechanism (Note S3). When the passivation completes and gets stabilized, the localized LiF/Li_2O indirect-SEI gets distributed across the interphase of Li^0, which persists throughout the cycling (Figure 2e). Collectively, LiF-induced SEI exhibits Li_2O-enriched SEI (Figure 1**d,e**, Figure 2**e-k**, **and** Note S4), temporal and chemical stability (Note S17 and Figure S13d), and improved electrochemical reversibility of Li^0 anode (Figure 5a and Figures S9−S11). These enhancements are afforded by the propensity of LiF forming the LiF/Li_2O grain boundaries[45] (Figure 3d), Li_2O-rich[40,51,52] and enhanced distribution of LiF/Li_2O indirect-SEI (Figure 1**d,e**, Figure 2**e-k**, **and** Note S4), adsorbing Li^+ onto LiF surfaces (Figure 4**e-g**), and creating the weakly solvating environment (Note S14).

In this work, we performed a comprehensive study of LiF to unravel the effects of LiF on Li^0 anodes. The focus has been placed on observing the influence of LiF on the SEI evolution and discovering the relevant characteristics of LiF that contribute to enhanced electrochemical performance in Li^0 anodes. By integrating empirical and theoretical findings, we emphasize that the roles played by LiF in the SEI on Li^0 anode are closely associated with Li_2O. Specifically, the observed phenomenon of the enrichment of Li_2O in the SEI and the strong tendency of LiF to interface with Li_2O were highlighted as key attributes of LiF in improving the performance of Li^0 anode. Additionally, we found that LiF exhibits non-negligible solubility and can spontaneously dissolve-reprecipitate in the electrolyte upon its saturation, elucidating the lack of LiF appearance within compact-SEI and placement of LiF as the indirect-SEI component alongside Li_2O. By consolidating these critical discoveries, the projected working mechanism of LiF for Li^0 anodes is outlined in this work. We envision that the content reported in this study can be leveraged to galvanize the advancements in SEI designs and understandings (Note S18) that propel Li^0 batteries closer to practical applications.

■ ASSOCIATED CONTENT

Supporting Information

The Supporting Information is available free of charge at https://pubs.acs.org/doi/10.1021/acs.nanolett.5c03437.

> Experimental details for materials, cryo-TEM/STEM, cryo-STEM EELS, SEM/EDXS, XRD, XPS, zeta potential, DFT/MD simulations, QCM, electrolyte solvation energies, ^{7}Li NMR, electrochemical measurements; Analyses of Li_2O passivation mechanism, DFT modeling, solubility, molecular dynamics, and electrochemical behavior of LiF; Supporting figures for LiF SE, cryo-STEM EELS analysis on rSEI LiF SE, DFT/MD analyses on LiF structures and surface interactions with electrolyte species, and electrochemical performance of RE and LiF SE (PDF)

■ AUTHOR INFORMATION

Corresponding Authors

Zhenan Bao − *Department of Chemical Engineering, Stanford University, Stanford, California 94305, United States;* orcid.org/0000-0002-0972-1715; Email: zbao@stanford.edu

Yi Cui − *Department of Materials Science and Engineering and Department of Energy Science and Engineering, Stanford University, Stanford, California 94305, United States; Stanford Institute for Materials and Energy Sciences, SLAC National Accelerator Laboratory, Menlo Park, California 94025, United States;* orcid.org/0000-0002-6103-6352; Email: yicui@stanford.edu

Authors

Mun Sek Kim − *Department of Materials Science and Engineering and Department of Chemical Engineering, Stanford University, Stanford, California 94305, United States; School of Mechanical and Aerospace Engineering, Nanyang Technological University, Singapore 639798, Singapore;* orcid.org/0000-0003-0918-3870

Jingyang Wang − *Department of Materials Science and Engineering, Stanford University, Stanford, California 94305, United States; Materials Sciences Division, Lawrence Berkeley Laboratory, Berkeley, California 94720, United States; Key Laboratory of Theoretical & Computational Photochemistry of Ministry of Education, College of Chemistry, Beijing Normal University, Beijing 100875, China;* orcid.org/0000-0003-3307-5132

Wenbo Zhang − *Department of Materials Science and Engineering, Stanford University, Stanford, California 94305, United States;* orcid.org/0000-0002-0828-594X

Philaphon Sayavong − *Department of Chemistry, Stanford University, Stanford, California 94305, United States;* orcid.org/0000-0001-7605-8194

Zewen Zhang − *Department of Materials Science and Engineering, Stanford University, Stanford, California 94305, United States;* orcid.org/0000-0002-4909-4330

Solomon T. Oyakhire − *Department of Chemical Engineering, Stanford University, Stanford, California 94305, United States*

Sanzeeda Baig Shuchi − *Department of Chemical Engineering, Stanford University, Stanford, California 94305, United States*

Sang Cheol Kim − *Department of Materials Science and Engineering, Stanford University, Stanford, California 94305, United States;* orcid.org/0000-0002-1749-8277

Yi Cui − *Department of Materials Science and Engineering, Stanford University, Stanford, California 94305, United States*

Yuelang Chen − *Department of Chemical Engineering and Department of Chemistry, Stanford University, Stanford, California 94305, United States;* orcid.org/0000-0002-5249-0596

Zhiao Yu − *Department of Chemical Engineering and Department of Chemistry, Stanford University, Stanford, California 94305, United States*

Huaxin Gong − *Department of Chemical Engineering, Stanford University, Stanford, California 94305, United States;* orcid.org/0000-0002-2493-0793

Rong Xu − *Department of Materials Science and Engineering, Stanford University, Stanford, California 94305, United States;* orcid.org/0000-0002-3694-595X

Junyoung Lee − *Department of Materials Science and Engineering, Stanford University, Stanford, California 94305, United States;* orcid.org/0009-0009-9903-2654

Il Rok Choi — *Department of Materials Science and Engineering and Department of Chemical Engineering, Stanford University, Stanford, California 94305, United States*

Jun Ho Lee — *Department of Materials Science and Engineering, Stanford University, Stanford, California 94305, United States*

Kristin A. Persson — *Department of Materials Science and Engineering, University of California, Berkeley, California 94720, United States; Energy Technologies Area, Lawrence Berkeley Laboratory, Berkeley, California 94720, United States;* orcid.org/0000-0003-2495-5509

Jian Qin — *Department of Chemical Engineering, Stanford University, Stanford, California 94305, United States;* orcid.org/0000-0001-6271-068X

Complete contact information is available at:
https://pubs.acs.org/10.1021/acs.nanolett.5c03437

Author Contributions

[⬒] These authors contributed equally: Mun Sek Kim, Jingyang Wang, and Wenbo Zhang.

Notes

The authors declare no competing financial interest.

ACKNOWLEDGMENTS

We acknowledge support from the Assistant Secretary for Energy Efficiency and Renewable Energy, Office of Vehicle Technologies of the US Department of Energy under the Battery Materials Research (BMR) Program and Battery 500 Consortium. Part of this work was performed at the Stanford Nano Shared Facilities (SNSF), supported by the National Science Foundation under award ECCS-2026822. Y. Cui (coauthor) acknowledges cryo-EM support from the US Department of Energy, Office of Basic Energy Sciences, Division of Materials Science and Engineering under contract DE-AC02-76SF00515.

REFERENCES

(1) Meng, Y. S.; Srinivasan, V.; Xu, K. Designing Better Electrolytes. *Science.* **2022**, *378*, 1–8.

(2) Adenusi, H.; Chass, G. A.; Passerini, S.; Tian, K. V.; Chen, G. Lithium Batteries and the Solid Electrolyte Interphase (SEI)—Progress and Outlook. *Adv. Energy Mater.* **2023**, *13*, 2203307.

(3) Li, Z.; Chen, Y.; Yun, X.; Gao, P.; Zheng, C.; Xiao, P. Critical Review of Fluorinated Electrolytes for High-Performance Lithium Metal Batteries. *Adv. Funct Mater.* **2023**, *33*, 2300502.

(4) Tan, J.; Matz, J.; Dong, P.; Shen, J.; Ye, M. A Growing Appreciation for the Role of LiF in the Solid Electrolyte Interphase. *Adv. Energy Mater.* **2021**, *11*, 2100046.

(5) Guo, R.; Kim, K.-H.; Gallant, B. M. Impact of LiF Particle Morphology on Overpotential and Structure of Li Metal Deposition. *J. Electrochem. Soc.* **2022**, *169*, 100523.

(6) He, M.; Guo, R.; Hobold, G. M.; Gao, H.; Gallant, B. M. The Intrinsic Behavior of Lithium Fluoride in Solid Electrolyte Interphases on Lithium. *Appl. Phys. Sci.* **2019**, *117* (1), 73–79, DOI: 10.1073/pnas.1911017116.

(7) Guo, R.; Gallant, B. M. Li2O Solid Electrolyte Interphase: Probing Transport Properties at the Chemical Potential of. *Lithium.* **2020**, *32*, 5525–5533.

(8) Huang, W.; Wang, H.; Boyle, D. T.; Li, Y.; Cui, Y. Resolving Nanoscopic and Mesoscopic Heterogeneity of Fluorinated Species in Battery Solid-Electrolyte Interphases by Cryogenic Electron Microscopy. *ACS Energy Lett.* **2020**, *5*, 1128–1135.

(9) Jagger, B.; Pasta, M. Solid Electrolyte Interphases in Lithium Metal Batteries. *Joule.* **2023**, *7*, 2228–2244.

(10) Fan, X.; Ji, X.; Han, F.; Yue, J.; Chen, J.; Chen, L.; Deng, T.; Jiang, J.; Wang, C. Fluorinated Solid Electrolyte Interphase Enables Highly Reversible Solid-State Li Metal Battery. *Sci. Adv.* **2018**, *4*, eaau9245.

(11) Zhao, Q.; Stalin, S.; Archer, L. A. Stabilizing Metal Battery Anodes through the Design of Solid Electrolyte Interphases. *Joule.* **2021**, *5*, 1119–1142.

(12) Liu, S.; Ji, X.; Yue, J.; Hou, S.; Wang, P.; Cui, C.; Chen, J.; Shao, B.; Li, J.; Han, F.; Tu, J.; Wang, C. High Interfacial-Energy Interphase Promoting Safe Lithium Metal Batteries. *J. Am. Chem. Soc.* **2020**, *142*, 2438–2447.

(13) Richards, W. D.; Miara, L. J.; Wang, Y.; Kim, J. C.; Ceder, G. Interface Stability in Solid-State Batteries. *Chem. Mater.* **2016**, *28* (1), 266–273, DOI: 10.1021/acs.chemmater.5b04082.

(14) Yildirim, H.; Kinaci, A.; Chan, M. K. Y.; Greeley, J. P. First-Principles Analysis of Defect Thermodynamics and Ion Transport in Inorganic SEI Compounds: LiF and NaF. *ACS Appl. Mater. Interfaces.* **2015**, *7*, 18985–18996.

(15) Xie, J.; Liao, L.; Gong, Y.; Li, Y.; Shi, F.; Pei, A.; Sun, J.; Zhang, R.; Kong, B.; Subbaraman, R.; Christensen, J.; Cui, Y. Stitching H-BN by Atomic Layer Deposition of LiF as a Stable Interface for Lithium Metal Anode. *Sci. Adv.* **2017**, *3*, No. eaao3170.

(16) Hobold, G. M.; Wang, C.; Steinberg, K.; Li, Y.; Gallant, B. M. High Lithium Oxide Prevalence in the Lithium Solid–Electrolyte Interphase for High Coulombic Efficiency. *Nat. Energy.* **2024**, *9*, 580–591.

(17) Zhang, Z.; Cui, Y.; Vila, R.; Li, Y.; Zhang, W.; Zhou, W.; Chiu, W.; Cui, Y. Cryogenic Electron Microscopy for Energy Materials. *Acc. Chem. Res.* **2021**, *54*, 3505–3517.

(18) Zhang, Z.; Li, Y.; Xu, R.; Zhou, W.; Li, Y.; Oyakhire, S. T.; Wu, Y.; Xu, J.; Wang, H.; Yu, Z.; Boyle, D. T.; Huang, W.; Ye, Y.; Chen, H.; Wan, J.; Bao, Z.; Chiu, W.; Cui, Y. Capturing the Swelling of Solid-Electrolyte Interphase in Lithium Metal Batteries. *Science.* **2022**, *375*, 66–70.

(19) Zachman, M. J.; Tu, Z.; Choudhury, S.; Archer, L. A.; Kourkoutis, L. F. Cryo-STEM Mapping of Solid–Liquid Interfaces and Dendrites in Lithium-Metal Batteries. *Nature.* **2018**, *560*, 345–349.

(20) Li, Y.; Li, Y.; Pei, A.; Yan, K.; Sun, Y.; Wu, C. L.; Joubert, L. M.; Chin, R.; Koh, A. L.; Yu, Y.; Perrino, J.; Butz, B.; Chu, S.; Cui, Y. Atomic Structure of Sensitive Battery Materials and Interfaces Revealed by Cryo–Electron Microscopy. *Science.* **2017**, *358*, 506–510.

(21) Tan, Y. H.; Lu, G. X.; Zheng, J. H.; Zhou, F.; Chen, M.; Ma, T.; Lu, L. L.; Song, Y. H.; Guan, Y.; Wang, J.; Liang, Z.; Xu, W. S.; Zhang, Y.; Tao, X.; Yao, H. B. Lithium Fluoride in Electrolyte for Stable and Safe Lithium-Metal Batteries. *Adv. Mater.* **2021**, *33* (42), 2102134 DOI: 10.1002/adma.202102134.

(22) Jurng, S.; Brown, Z. L.; Kim, J.; Lucht, B. L. Effect of Electrolyte on the Nanostructure of the Solid Electrolyte Interphase (SEI) and Performance of Lithium Metal Anodes. *Energy Environ. Sci.* **2018**, *11*, 2600–2608.

(23) Boyle, D. T.; Huang, W.; Wang, H.; Li, Y.; Chen, H.; Yu, Z.; Zhang, W.; Bao, Z.; Cui, Y. Corrosion of Lithium Metal Anodes during Calendar Ageing and Its Microscopic Origins. *Nat. Energy.* **2021**, *6*, 487–494.

(24) Brown, Z. L.; Jurng, S.; Nguyen, C. C.; Lucht, B. L. Effect of Fluoroethylene Carbonate Electrolytes on the Nanostructure of the Solid Electrolyte Interphase and Performance of Lithium Metal Anodes. *ACS Appl. Energy Mater.* **2018**, *1*, 3057–3062.

(25) Weng, S.; Zhang, X.; Yang, G.; Zhang, S.; Ma, B.; Liu, Q.; Liu, Y.; Peng, C.; Chen, H.; Yu, H.; Fan, X.; Cheng, T.; Chen, L.; Li, Y.; Wang, Z.; Wang, X. Temperature-Dependent Interphase Formation and Li+ Transport in Lithium Metal Batteries. *Nat. Commun.* **2023**, *14*, 4474.

(26) Han, B.; Li, X.; Bai, S.; Zou, Y.; Lu, B.; Zhang, M.; Ma, X.; Chang, Z.; Meng, Y. S.; Gu, M. Conformal Three-Dimensional

Interphase of Li Metal Anode Revealed by Low-Dose Cryoelectron Microscopy. *Matter.* **2021**, *4*, 3741−3752.

(27) Zhang, K.; Wu, F.; Wang, X.; Zheng, L.; Yang, X.; Zhao, H.; Sun, Y.; Zhao, W.; Bai, Y.; Wu, C. An Ion-Dipole-Reinforced Polyether Electrolyte with Ion-Solvation Cages Enabling High−Voltage-Tolerant and Ion-Conductive Solid-State Lithium Metal Batteries. *Adv. Funct Mater.* **2022**, *32*, 2107764.

(28) Sun, C.; Li, R.; Weng, S.; Zhu, C.; Chen, L.; Jiang, S.; Li, L.; Xiao, X.; Liu, C.; Chen, L.; Deng, T.; Wang, X.; Fan, X. Reduction-Tolerance Electrolyte Design for High-Energy Lithium Batteries. *Angew. Chem. Int. Ed.* **2024**, *63*, No. e202400761, DOI: 10.1002/anie.202400761.

(29) Liu, Y.; Tao, X.; Wang, Y.; Jiang, C.; Ma, C.; Sheng, O.; Lu, G.; Lou, X. W. D. Self-Assembled Monolayers Direct a LiF-Rich Interphase toward Long-Life Lithium Metal Batteries. *Science.* **2022**, *375*, 739−745.

(30) Chen, Z.; Wang, B.; Li, Y.; Bai, F.; Zhou, Y.; Li, C.; Li, T. Stable Solvent-Derived Inorganic-Rich Solid Electrolyte Interphase (SEI) for High-Voltage Lithium-Metal Batteries. *ACS Appl. Mater. Interfaces.* **2022**, *14*, 28014−28020.

(31) Yu, Z.; Rudnicki, P. E.; Zhang, Z.; Huang, Z.; Celik, H.; Oyakhire, S. T.; Chen, Y.; Kong, X.; Kim, S. C.; Xiao, X.; Wang, H.; Zheng, Y.; Kamat, G. A.; Kim, M. S.; Bent, S. F.; Qin, J.; Cui, Y.; Bao, Z. Rational Solvent Molecule Tuning for High-Performance Lithium Metal Battery Electrolytes. *Nat. Energy.* **2022**, *7*, 94−106.

(32) Yu, Z.; Wang, H.; Kong, X.; Huang, W.; Tsao, Y.; Mackanic, D. G.; Wang, K.; Wang, X.; Huang, W.; Choudhury, S.; Zheng, Y.; Amanchukwu, C. V.; Hung, S. T.; Ma, Y.; Lomeli, E. G.; Qin, J.; Cui, Y.; Bao, Z. Molecular Design for Electrolyte Solvents Enabling Energy-Dense and Long-Cycling Lithium Metal Batteries. *Nat. Energy.* **2020**, *5*, 526−533.

(33) Kim, S. C.; Wang, J.; Xu, R.; Zhang, P.; Chen, Y.; Huang, Z.; Yang, Y.; Yu, Z.; Oyakhire, S. T.; Zhang, W.; Greenburg, L. C.; Kim, M. S.; Boyle, D. T.; Sayavong, P.; Ye, Y.; Qin, J.; Bao, Z.; Cui, Y. High-Entropy Electrolytes for Practical Lithium Metal Batteries. *Nat. Energy.* **2023**, *8*, 814−826.

(34) Wang, H.; Yu, Z.; Kong, X.; Kim, S. C.; Boyle, D. T.; Qin, J.; Bao, Z.; Cui, Y. Liquid Electrolyte: The Nexus of Practical Lithium Metal Batteries. *Joule.* **2022**, *6*, 588−616.

(35) Kim, S. C.; Kong, X.; Vilá, R. A.; Huang, W.; Chen, Y.; Boyle, D. T.; Yu, Z.; Wang, H.; Bao, Z.; Qin, J.; Cui, Y. Potentiometric Measurement to Probe Solvation Energy and Its Correlation to Lithium Battery Cyclability. *J. Am. Chem. Soc.* **2021**, *143*, 10301−10308.

(36) Wu, H.; Jia, H.; Wang, C.; Zhang, J. G.; Xu, W. Recent Progress in Understanding Solid Electrolyte Interphase on Lithium Metal Anodes. *Adv. Energy Mater.* **2021**, *11*, 2003092.

(37) Yamada, Y.; Wang, J.; Ko, S.; Watanabe, E.; Yamada, A. Advances and Issues in Developing Salt-Concentrated Battery Electrolytes. *Nat. Energy.* **2019**, *4*, 269−280.

(38) Hobold, G. M.; Lopez, J.; Guo, R.; Minafra, N.; Banerjee, A.; Shirley Meng, Y.; Shao-Horn, Y.; Gallant, B. M. Moving beyond 99.9% Coulombic Efficiency for Lithium Anodes in Liquid Electrolytes. *Nat. Energy.* **2021**, *6*, 951−960.

(39) Li, Y.; Huang, W.; Li, Y.; Pei, A.; Boyle, D. T.; Cui, Y. Correlating Structure and Function of Battery Interphases at Atomic Resolution Using Cryoelectron Microscopy. *Joule.* **2018**, *2*, 2167−2177.

(40) Kim, M. S.; Zhang, Z.; Rudnicki, P. E.; Yu, Z.; Wang, J.; Wang, H.; Oyakhire, S. T.; Chen, Y.; Kim, S. C.; Zhang, W.; Boyle, D. T.; Kong, X.; Xu, R.; Huang, Z.; Huang, W.; Bent, S. F.; Wang, L. W.; Qin, J.; Bao, Z.; Cui, Y. Suspension Electrolyte with Modified Li+ Solvation Environment for Lithium Metal Batteries. *Nat. Mater.* **2022**, *21*, 445−454.

(41) Kim, M. S.; Zhang, Z.; Wang, J.; Oyakhire, S. T.; Kim, S. C.; Yu, Z.; Chen, Y.; Boyle, D. T.; Ye, Y.; Huang, Z.; Zhang, W.; Xu, R.; Sayavong, P.; Bent, S. F.; Qin, J.; Bao, Z.; Cui, Y. Revealing the Multifunctions of Li3N in the Suspension Electrolyte for Lithium Metal Batteries. *ACS Nano* **2023**, *17*, 3168−3180.

(42) Sina, M.; Nam, K. W.; Su, D.; Pereira, N.; Yang, X. Q.; Amatucci, G. G.; Cosandey, F. Structural Phase Transformation and Fe Valence Evolution in FeO XF2-x/C Nanocomposite Electrodes during Lithiation and de-Lithiation Processes. *J. Mater. Chem. A Mater.* **2013**, *1*, 11629−11640.

(43) Zheng, J.; Ju, Z.; Zhang, B.; Nai, J.; Liu, T.; Liu, Y.; Xie, Q.; Zhang, W.; Wang, Y.; Tao, X. Lithium Ion Diffusion Mechanism on the Inorganic Components of the Solid-Electrolyte Interphase. *J. Mater. Chem. A Mater.* **2021**, *9*, 10251−10259.

(44) Piao, N.; Liu, S.; Zhang, B.; Ji, X.; Fan, X.; Wang, L.; Wang, P. F.; Jin, T.; Liou, S. C.; Yang, H.; Jiang, J.; Xu, K.; Schroeder, M. A.; He, X.; Wang, C. Lithium Metal Batteries Enabled by Synergetic Additives in Commercial Carbonate Electrolytes. *ACS Energy Lett.* **2021**, *6*, 1839−1848.

(45) Ramasubramanian, A.; Yurkiv, V.; Foroozan, T.; Ragone, M.; Shahbazian-Yassar, R.; Mashayek, F. Lithium Diffusion Mechanism through Solid-Electrolyte Interphase in Rechargeable Lithium Batteries. *J. Phys. Chem. C.* **2019**, *123* (16), 10237−10245, DOI: 10.1021/acs.jpcc.9b00436.

(46) Lu, Y.; Tu, Z.; Archer, L. A. Stable Lithium Electrodeposition in Liquid and Nanoporous Solid Electrolytes. *Nat. Mater.* **2014**, *13*, 961−969.

(47) Ozhabes, Y.; Gunceler, D.; Arias, T. A. Stability and Surface Diffusion at Lithium-Electrolyte Interphases with Connections to Dendrite Suppression. *arXiv*2015. DOI: 10.48550/arXiv.1504.05799

(48) Sayavong, P.; Zhang, W.; Oyakhire, S. T.; Boyle, D. T.; Chen, Y.; Kim, S. C.; Vilá, R. A.; Holmes, S. E.; Kim, M. S.; Bent, S. F.; Bao, Z.; Cui, Y. Dissolution of the Solid Electrolyte Interphase and Its Effects on Lithium Metal Anode Cyclability. *J. Am. Chem. Soc.* **2023**, *145*, 12342−12350.

(49) Xia, Y.; Zhou, P.; Kong, X.; Tian, J.; Zhang, W.; Yan, S.; Hou, W. H.; Zhou, H. Y.; Dong, H.; Chen, X.; Wang, P.; Xu, Z.; Wan, L.; Wang, B.; Liu, K. Designing an Asymmetric Ether-like Lithium Salt to Enable Fast-Cycling High-Energy Lithium Metal Batteries. *Nat. Energy.* **2023**, *8*, 934−945.

(50) Boyle, D. T.; Kong, X.; Pei, A.; Rudnicki, P. E.; Shi, F.; Huang, W.; Bao, Z.; Qin, J.; Cui, Y. Transient Voltammetry with Ultramicroelectrodes Reveals the Electron Transfer Kinetics of Lithium Metal Anodes. *ACS Energy Lett.* **2020**, *5*, 701−709.

(51) Li, Y.; Liu, Q.; Wu, S.; Geng, L.; Popovic, J.; Li, Y.; Chen, Z.; Wang, H.; Wang, Y.; Dai, T.; Yang, Y.; Sun, H.; Lu, Y.; Zhang, L.; Tang, Y.; Xiao, R.; Li, H.; Chen, L.; Maier, J.; Huang, J.; Hu, Y. S. Unraveling the Reaction Mystery of Li and Na with Dry Air. *J. Am. Chem. Soc.* **2023**, *145*, 10576−10583.

(52) Lee, J.; Kim, M. S.; Cui, Y.; Zhang, W.; Shuchi, S. B.; Holmes, S. E.; Lee, J. H.; Serrao, C.; Kim, S. C.; Holoubek, J.; Sayavong, P.; Cai, A.; Choi, I. R.; Cui, Y. Reactive Suspension Electrolytes for Lithium Metal Batteries. *ACS Energy Lett.* **2025**, *10*, 4252−4259.